Elastic instabilities in crystals from *ab initio* stress - strain relations

1997 J. Phys.: Condens. Matter 9 8579

(http://iopscience.iop.org/0953-8984/9/41/005)

J. Phys.: Condens. Matter **9** (1997) 8579–8589. Printed in the UK PII: S0953-8984(97)82644-6

Elastic instabilities in crystals from *ab initio* stress–strain relations

B B Karki, G J Ackland and J Crain

Department of Physics and Astronomy, The University of Edinburgh, Edinburgh EH9 3JZ, UK

Received 17 March 1997, in final form 1 August 1997

Abstract. Pressure-induced elastic instabilities are investigated in the prototypic ionic and covalent solids (MgO, CaO, SiO_2 and Si) using generalized elastic stability criteria based on the elastic stiffness coefficients (c_{ij}) which are determined directly from stress–strain relations. From first-principles computer simulations of the instabilities, we demonstrate the validity and importance of the generalized criteria relative to the conventional criteria in describing the crystal stability under hydrostatic pressure in relation to the real structural transformations. We examine systems for which the two phases can be related by a simple deformation, and in all cases we show that the generalized elastic stiffness coefficient associated with that deformation softens toward the transition. The shear stability criterion ($c_{44} > 0$) bounds the first-order B1–B2 phase transition pressure from above and below in MgO and CaO, suggesting a wide pressure regime of metastability, whereas the tetragonal shear stability criterion ($(c_{11} - c_{12})/2 > 0$) predicts precisely the second-order rutile-to-$CaCl_2$ transition in SiO_2. The high-pressure elastic behaviour of diamond structure Si is studied in detail. A tetragonal shear instability corresponding to its transformation to the β-Sn structure should occur in diamond structure Si at a pressure of 101 GPa, compared to the experimental value of 9 to 13 GPa for the transition pressure.

1. Introduction

Mechanical stability of homogeneous crystals has long been a subject of extensive theoretical and computational investigation. Born initiated the systematic study of crystal stability under load [1]. The well-known Born stability criteria are a set of conditions on the elastic constants (C_{ij}) which are related to the second-order change in the internal energy of a crystal under deformation. Later, Hill and Milstein suggested that the convexity of the internal energy in a crystal under stress is coordinate dependent and hence the ranges of Born stability are strongly sensitive to the choice of coordinates [2–4]. By considering the external work done to second order (i.e. in a classical treatment), they found significant quantitative and qualitative differences in the ranges of Born and classical stability [5]. However, they did not point out clearly the fact that the Born conditions are valid only for the special case of zero stress.

It has been recently suggested that the Born conditions are valid only for the stability analysis of an unstressed lattice and not for the stressed lattice [6, 7]. The stability criteria have been formulated in terms of the elastic stiffness coefficients (c_{ij}) which govern the proper stress–strain relations at finite strain by considering both the internal energy and the external work done during deformation [6, 7]. This suggests that the stability analyses depend mainly on a proper generalization of the zero-stress elastic constants valid for arbitrary stress [8, 9]. The generic features of these criteria relative to the conventional

0953-8984/97/418579+11$19.50

criteria have been demonstrated successfully for the cases of hydrostatic tension and compression, uniaxial tension, and lattice expansion by molecular dynamics simulations [6, 7]. However, there exist relatively few demonstrations of precise identification of the elastic instability which are closely related to the structural transformation. A tetragonal shear instability was suggested to be associated with the pressure-induced phase transition in silicon from the diamond structure to the β-Sn structure [10]. Similarly a shear instability was predicted to cause amorphization in zinc-blende structure SiC under hydrostatic compression [11].

In all of the previous demonstrations [6, 7, 10, 11] of the validity and importance of the generalized elastic stability criteria for arbitrary stress, the elastic constants (C_{ij}) were first calculated and their values were used to estimate the elastic stiffness coefficients (c_{ij}) which were, in turn, used to determine the instability of the crystal. Here we calculate these coefficients (c_{ij}) directly from stress–strain relations [8, 12, 13]. More applications of these stability criteria are required in systems where the elastic instabilities suggested by the stability criteria can be related directly to the structural phase transitions.

We have recently determined the high-pressure structural and elastic properties of three oxides, MgO, CaO and SiO_2, from first-principles computer simulations based on the plane-wave pseudopotential method within the local density approximation [12, 15]. The elastic stiffness coefficients (c_{ij}) calculated from stress–strain relations under external pressure [12] are the appropriate elastic quantities (equivalent to B_{ij} used in reference [6, 7, 9]) which enter into the generalized stability criteria. Also, enthalpy (zero-temperature free energy) considerations suggest that MgO and CaO should transform from the low-pressure rock-salt (B1) structure to the high-pressure CsCl (B2) structure at pressures of 451 and 58 GPa, respectively, whereas SiO_2 shows a structural transformation from the tetragonal rutile phase (stishovite) to the orthorhombic $CaCl_2$ phase at about 47 GPa. Here we extend these high-pressure elasticity calculations further and analyse the pressure-induced elastic instabilities in these systems (MgO, CaO and SiO_2) and also in diamond structure Si in relation to the pressure-induced structural transformations.

2. Elastic stability criteria

The well-known Born elastic stability criteria can be derived by expanding the internal energy in the strain and by requiring convexity of the energy [1]. Three generally accepted elastic stability criteria for a cubic crystal [6, 9] are

$$C_{11} + 2C_{12} > 0 \qquad C_{44} > 0 \qquad C_{11} - C_{12} > 0 \tag{1}$$

which are connected to the bulk, shear and tetragonal shear moduli respectively and are referred to as spinodal, shear and Born criteria, respectively. Here the C_{ij} are the elastic constant tensors (in Voigt notation) which are derived from the change in the internal energy under deformation.

The Born elastic stability criteria have been shown to be valid only for the special case of zero stress. The generalization of the stability criteria to the non-zero-stress case can be done by formulating the stability conditions in terms of the elastic stiffness coefficients which govern the proper stress–strain relations at finite strains [6, 7, 9]. The relevant elastic stiffness tensor c_{ijkl} (which is denoted by B_{ijkl} in references [6, 7, 9]) is defined as

$$c_{ijkl} = \left(\frac{\partial \sigma_{ij}(\boldsymbol{x})}{\partial e_{kl}}\right)_X \tag{2}$$

where σ_{ij} and e_{kl} are the applied stress and Eulerian strain tensors, and $\boldsymbol{X}$ and $\boldsymbol{x}$ are the coordinates before and after the deformation. For the case of isotropic stress (i.e. under

hydrostatic pressure P) [8, 9], we have

$$c_{ijkl} = C_{ijkl} + \frac{P}{2}(2\delta_{ij}\delta_{kl} - \delta_{il}\delta_{jk} - \delta_{ik}\delta_{jl}) \tag{3}$$

where

$$C_{ijkl} = \left(\frac{1}{V(\boldsymbol{x})}\frac{\partial^2 E(\boldsymbol{x})}{\partial e_{ij}\,\partial e_{kl}}\right)_X. \tag{4}$$

The notation C_{ijkl} used here to denote the second-order derivatives with respect to the infinitesimal strain (Eulerian) variables should not be confused with the same notation used by several authors [7, 8, 9] to represent the elastic constants defined with respect to the finite-strain (Lagrange) coordinates. It should be noted that the elastic stiffnesses c_{ijkl} are independent of the choice of strain variables. The elastic stiffness tensor c_{ijkl} provides a generalization of the zero-stress elastic constant tensor valid under arbitrary stress [8].

For a cubic crystal under hydrostatic pressure, the generalized elastic stability criteria [6, 7] in analogy to the conventional criteria (equation (1)) are

$$c_{11} + 2c_{12} > 0 \qquad c_{44} > 0 \qquad c_{11} - c_{12} > 0. \tag{5}$$

In the case of hydrostatic pressure, the c_{ij} (in Voigt notation) are related to the C_{ij} defined with respect to the Eulerian strain variables by

$$c_{11} = C_{11} \qquad c_{12} = C_{12} + P \qquad c_{44} = C_{44} - \frac{P}{2}. \tag{6}$$

The finite-load stability conditions (equation (5)) for a cubic crystal reduce to the Born stability criteria in the limit of vanishing load.

3. Computational details

The calculations are performed using the plane-wave pseudopotential method within the local density approximation (LDA) [15]. The optimized, norm-conserving, non-local pseudopotentials generated by the Q_C-tuning method are used [16, 17]. The finite plane-wave basis-set corrections [18] to total energies and stresses are included so that the corrected total energy and stress differences are converged to better than 0.1 meV and 0.02 GPa per unit formula respectively. These details for MgO, CaO and SiO_2 have been given elsewhere [12, 14]. For silicon, a plane-wave basis set with a 300 eV cut-off is used to expand the electronic wavefunctions at ten special k-points [19]. The Pulay stress is about 0.6 GPa at equilibrium volume. A higher number of k-points are required in the case of the deformed lattices to derive elastic moduli. The appropriate symmetry of the crystal structure is enforced on the electronic charge density and wavefunctions throughout the simulations.

For a given isotropic pressure P, the total stress is

$$\sigma_{ij} = \sigma_{ij}^c + \sigma_P - P \qquad (i, j = 1, 2, 3) \tag{7}$$

where σ_{ij}^c is the self-consistent stress tensor [20] and σ_P is the isotropic Pulay stress [18]. The elastic stiffness coefficients (c_{ij}) are determined from the computation of the stresses generated by small deformations of the equilibrium unit cell (equation (2)). It is more direct to calculate the elastic moduli using stress–strain relations than using strain-energy density. We vary the magnitude of the strain and derive the elastic moduli from the resulting (non-linear) stress–strain relation [12]. In order to include coupling between strains and vibrational modes, the ionic positions are re-optimized in the strained lattice.

4. Ionic compounds

4.1. MgO

On the basis of the thermodynamic criterion of equality of enthalpies ($H = E + PV$) at zero temperature, MgO is predicted to exhibit a pressure-induced structural transformation from the low-pressure NaCl structure (B1 phase) to the high-pressure CsCl structure (B2 phase) at 451 GPa [12]. This prediction is in consistent with the experimental observation that the B1 phase is stable, at least up to 230 GPa [21]. The exceptionally wide stability field of MgO makes study of its elastic instability an important test of the validity and importance of the finite-load stability criteria.

We have recently determined the three elastic stiffness coefficients, c_{11}, c_{12} and c_{44}, of the B1 structure MgO from the stress–strain relations up to 150 GPa [12]. Here, we calculate these quantities over a much wider pressure range to study elastic instability in MgO. Both bulk ($(c_{11} + 2c_{12})/3$) and tetragonal shear ($(c_{11} - c_{12})/2$) moduli increase strongly with pressure suggesting that the B1 structure MgO is increasingly stable against spinodal and tetragonal shear deformations. However, as shown in figure 1(a), c_{44} increases initially with increasing pressure, becomes maximum at about 350 GPa, then decreases gradually to zero at about 1400 GPa, and thereafter becomes increasingly negative. This implies that a shear instability should occur in the B1 phase of MgO at around 1400 GPa.

The following shear strain:

$$\epsilon = -\begin{pmatrix} 0 & e & e \\ e & 0 & e \\ e & e & 0 \end{pmatrix} \tag{8}$$

is used to evaluate c_{44}. Here, the strained lattice vectors $\boldsymbol{a}'$ are related to unstrained vectors $\boldsymbol{a}$ by $\boldsymbol{a}' = (\mathbf{I} + \epsilon)\boldsymbol{a}$, where $\mathbf{I}$ is the identity matrix. If the initial lattice is B1, then a strain of $e = 0.2$ effects a transformation to B2 phase.

To test this stability we deform the primitive cell of the B1 phase with a small shear strain ($e = 0.01$) defined by equation (8) at several pressures up to 1600 GPa and test whether the applied strain grows under structural (cell) relaxation following the *ab initio* constant-pressure relaxation method [22]. At all pressures below 1400 GPa, the deformed lattice regains its original (B1) phase (i.e. e decreases from 0.01 to 0.0) whereas at pressures above 1400 GPa, the applied strain grows eventually to the value of $e = 0.2$. This shows that the shear instability should occur at around 1400 GPa; this is the pressure at which c_{44} vanishes, consistent with the prediction of the generalized stability criteria.

In analogy to the shear instability which occurs in the B1 phase in MgO under compression, one should expect a similar instability in the B2 phase under decompression. As illustrated in figure 1(a), the elastic constant c_{44} of B2 structure MgO vanishes at about 57 GPa. The instability in the B2 lattice at 57 GPa under decompression (release of the applied pressure) is supported by the structural simulation of the slightly deformed cubic primitive cell of the B2 phase with the shear strain (equation (8)) at several pressures.

The value of the elastic constant C_{44} of the B1 phase derived from the internal energy ($\Delta E/V = 6C_{44}e^2$), does not soften with pressure (figure 1(a)) indicating the absence of the shear instability in MgO (unless it occurs at relatively much higher pressure). However, C_{44} of the B2 phase vanishes at about 37 GPa which is below the pressure of 57 GPa at which c_{44} is zero, and the simulation of the instability supports the value of 57 GPa. The stability limit of MgO predicted by the generalized criterion ($c_{44} > 0$) which differs significantly from that predicted by the conventional criterion ($C_{44} > 0$) is consistent with the structural simulation.

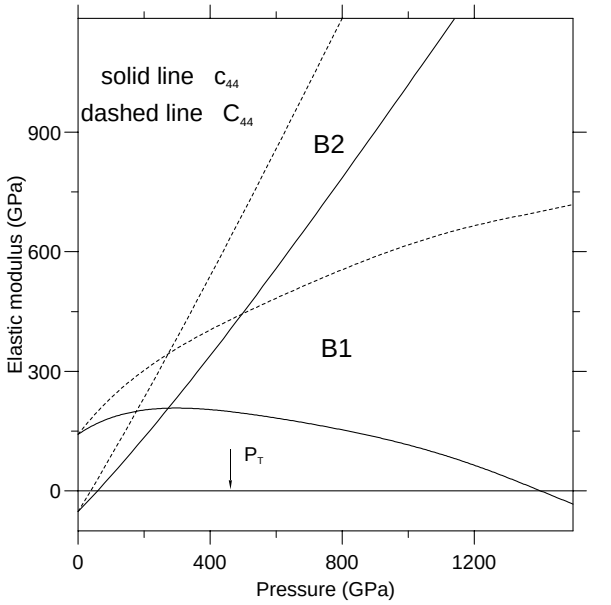

(a)

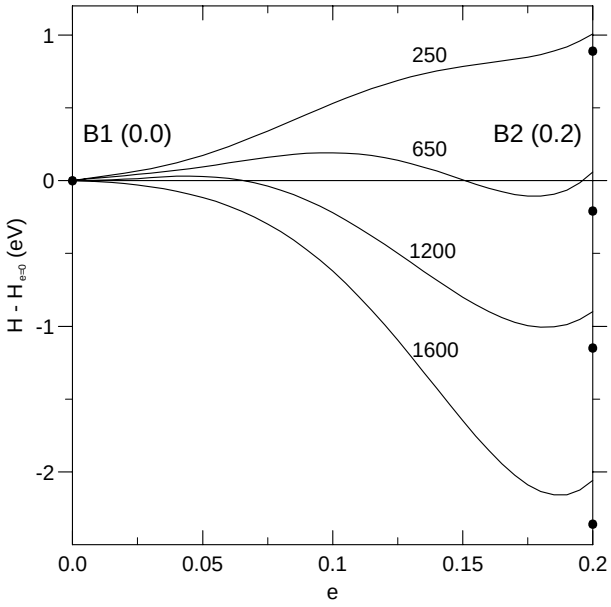

(b)

Figure 1. (a) The pressure variation of c_{44} and C_{44} for the B1 and B2 phases of MgO. The arrow indicates the B1–B2 transition pressure (P_T) predicted by thermodynamic equality of enthalpies. (b) The relative enthalpy of the deformed B1 structure of MgO versus the shear strain (e) at different pressures (indicated by numbers, in GPa). The solid circles represent the relative enthalpies of the optimized structures. Note that at $e = 0.2$, the strained B1 lattice has undergone a volume contraction of 10%, and thus represents B2 at a higher pressure.

When the magnitude of the strain, e, takes the value of 0.2 under simulation (at pressures

above 1400 GPa) of the slightly deformed B1 lattice with the shear strain (equation (8)), the resulting structure is equivalent to the B2 phase, i.e. the primitive cell becomes cubic. In other words, the rhombohedral primitive cell of the B1 phase ($Fm3m$ space group) can be changed into the cubic cell of the B2 phase ($Pm3m$ symmetry) by a compression along the body diagonal [111] direction, i.e. the change of symmetry can be induced by the shear deformation defined by equation (8). (The [110] direction in B1 becomes the [100] direction in B2, but the [111] direction connects the same atoms in both structures, and hence c_{44} is the relevant stiffness constant in each case.)

The softening of c_{44} in both phases suggests that the predicted shear instability in MgO may be related to a certain extent to the real B1–B2 phase transition mechanism. The elastic stiffness coefficient c_{44} of MgO remains high for both the B1 and B2 phases at the transition pressure of 451 GPa but it vanishes at pressures beyond the transition. This indicates that the elastic stability is insufficient to determine precisely the thermodynamic stability and hence the first-order B1–B2 phase transition in MgO. However, the elastic stability criterion can still be used to place bounds on the transition pressure for the first-order phase transition since the corresponding change of symmetry can be induced by an elastic instability [10].

The shear instability ($c_{44} = 0$) follows the B1–B2 phase transition along the specific reaction path of the homogeneous deformation which involves an activation barrier. We calculate the activation barrier along the reaction path described by the shear strain (equation (8)) from $e = 0.0$ (the B1 phase) to $e = 0.2$ (the equivalent B2 phase) at different pressures (figure 1(b)). The barrier is a measure of the relative enthalpy ($H - H_{e=0}$) of the deformed primitive cell of B1 structure MgO with respect to the unstrained cell ($e = 0.0$). At 250 GPa, both the strained lattice under $e = 0.2$ (i.e. equivalent to the B2 phase) and the optimized B2 phase possess higher energy than the optimized B1 phase does, making the B1 phase stable which is consistent with both elastic and thermodynamic criteria. At 650 GPa, a small activation barrier exists suggesting that the B1 phase is still elastically stable. However, the energies of both the equivalent and optimized B2 phases are slightly lower than that of the B1 phase. Correspondingly, the thermodynamic requirement of equality of free energies which ignores essentially the presence of a kinetic barrier predicts that the B1 phase should transform to the B2 phase at some pressure (i.e. at 451 GPa) between 250 and 650 GPa. As shown in figure 1(b), the barrier height decreases with increasing pressure, and both of the equivalent and optimized B2 phases become more stable energetically at higher pressures. Finally at much higher pressures (such as 1600 GPa) beyond 1400 GPa at which c_{44} becomes zero, the activation barrier associated with the shear strain vanishes. This implies that the shear instability should result in the structural transformation from the B1 to the B2 phase in MgO at those pressures. The elastic instability thus gives a higher transition pressure (1400 GPa) than the thermodynamic prediction of 451 GPa [12] for the case of the compression. On the other hand, for the case of the hydrostatic decompression of the B2 phase, the shear instability gives a lower pressure (57 GPa) than the free-energy prediction of 451 GPa. Thus, the elastic stability criteria should bound the pressure-induced B1–B2 phase transition in MgO from above and below.

4.2. CaO

We have recently found that the B1 phase of CaO becomes thermodynamically unstable at 58 GPa in excellent agreement with experimental observation at 53–70 GPa [23–25]. The value of c_{44} for the B1 phase as derived from the stress–strain relation vanishes at 177 GPa whereas that of the B2 phase becomes zero at -1.5 GPa (figure 2). These $c_{44} = 0$ conditions determine the shear instability in CaO and should correspond to the B1–B2

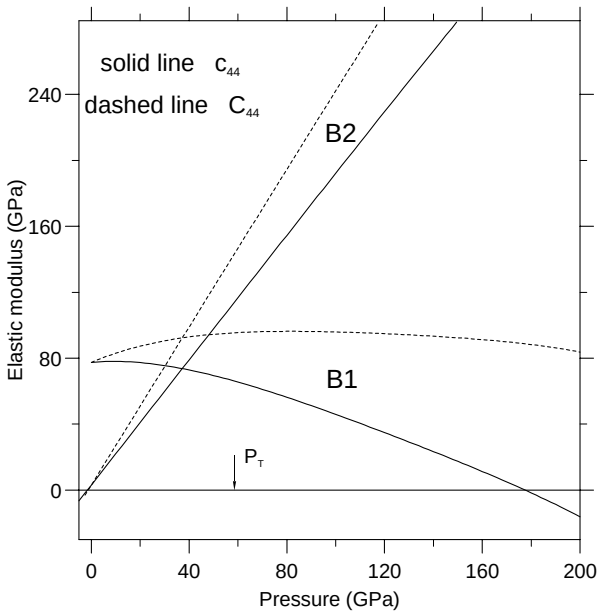

Figure 2. The pressure variations of c_{44} and C_{44} for B1 and B2 phases of CaO.

structural transformation in each direction at about 177 and -1.5 GPa, compared to the pressure of 58 GPa obtained by equating the enthalpies of the two phases. As in the case of MgO, the elastic stability criteria provide the upper (177 GPa) and lower (-1.5 GPa) bounds on the transition pressure of CaO. The large discrepancy between the transition pressures predicted by the elastic instability and thermodynamic criteria can be interpreted as the presence of a substantial activation barrier to this particular transition route.

The value for C_{44} for the B1 phase derived from ΔE remains high over the pressure range studied and is likely to vanish at much higher pressure, which is not consistent with the structural simulation of the instability (figure 2). However, both $c_{44} = 0$ and $C_{44} = 0$ should give similar values of the lower limit for the transition pressure since the relevant pressure is very close to zero (figure 2).

5. Covalent compounds

5.1. SiO_2

The structural transformation from the rutile phase (stishovite) to the $CaCl_2$ phase in SiO_2 serves as a good example of tetragonal shear instability under hydrostatic pressure. We have recently predicted that silica transforms from the tetragonal (rutile) to the orthorhombic ($CaCl_2$) phase at 47 GPa [14] in agreement with the Raman spectroscopic observation at 50 ± 3 GPa [33]. Figure 3 shows the pressure variation of the tetragonal shear modulus ($(c_{11} - c_{12})/2$) of both the rutile and $CaCl_2$ phases of silica. The modulus of the rutile structure silica softens slowly initially and more rapidly with increasing pressure, eventually vanishing at about 47 GPa at which pressure the tetragonal shear modulus of the $CaCl_2$ phase also vanishes with decreasing pressure. However, the modulus ($(C_{11} - C_{12})/2$) from the strain-energy density vanishes at about 49 and 45 GPa, respectively, for the rutile phase under compression and the $CaCl_2$ phase under decompression. It is to be noted that the

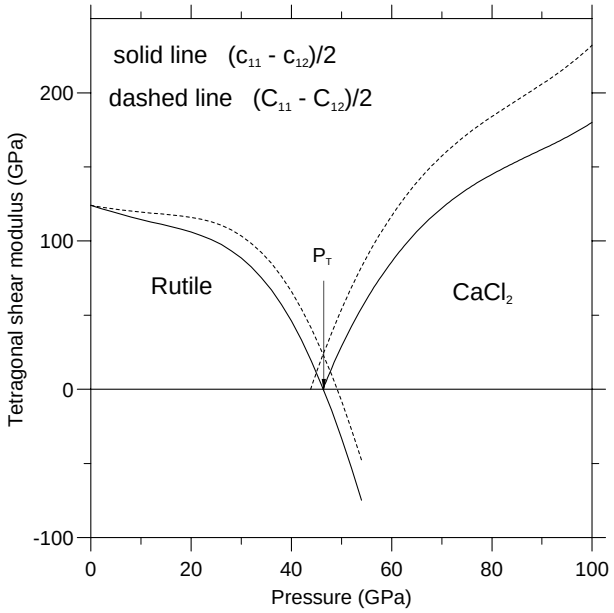

Figure 3. The pressure variation of the tetragonal shear moduli for rutile and $CaCl_2$ structure SiO_2.

calculated modulus ($(c_{11} - c_{12})/2$) does not soften with pressure unless the ions are allowed to relax in the deformed cell. Moreover, the frequency of the rutile B_{1g} mode vanishes at a much higher pressure of 86 GPa, so the B_{1g} mode would become unstable and induce the structural transformation of stishovite to $CaCl_2$ phase at this much higher pressure, compared to the actual pressure of 47 GPa. Thus, the rutile-to-$CaCl_2$ phase transition can be thought of as an elastic instability which arises from the strong coupling between elastic constants and the soft rutile B_{1g} mode [14].

We minimize the enthalpy with respect to the lattice parameters and ion positions of the orthorhombically strained unit cell of the rutile phase at several pressures. Under full structural optimization, at pressures of 0, 20 and 40 GPa, the strained unit cell finally relaxes back to the tetragonal (rutile) phase, whereas at 50 GPa and higher pressures it retains the orthorhombic ($CaCl_2$) phase. Thus full structural optimization of the strained tetragonal lattice of the rutile phase and orthorhombic lattice of the $CaCl_2$ phase at several pressures demonstrates that the elastic instability should occur at 47 GPa and cause the second-order rutile-to-$CaCl_2$ phase transition in silica. Unlike in the cases of MgO and CaO, both the thermodynamic and generalized elastic criteria predict exactly the same transition pressure since the tetragonal shear modulus actually vanishes at the transition point. In this case the elastic instability is the mechanism by which the transformation occurs. Both the upper and lower bounds on the transition pressure suggested by the criteria based on the conventional elastic constants are found to be inconsistent with the structural simulation and also with thermodynamic prediction.

5.2. Si

A number of experimental and theoretical investigations have found that silicon transforms from the diamond–cubic structure to a tetragonal β-Sn structure at 9 to 13 GPa [10, 26, 27].

Table 1. The lattice constant a (in Å), elastic stiffness coefficients c_{ij} (in GPa), isotropic bulk and shear moduli, K and G respectively (in GPa), and elastic anisotropy factor $A = 1 - 2c_{44}/(c_{11} - c_{12})$ of diamond structure Si.

P (GPa)	a	c_{11}	c_{12}	c_{44}	K	G	A
0	5.3926	165.6	66.9	77.2	99.8	64.5	0.564
*	5.4310	167.5	65.0	80.1	99.2	67.0	0.563
2	5.3569	175.4	77.0	78.4	109.8	65.0	0.593
5	5.3081	186.1	89.8	79.3	121.9	64.9	0.647
10	5.2374	204.4	110.3	80.1	141.7	64.7	0.702
15	5.1773	220.6	130.0	79.4	160.2	63.4	0.753

* Experimental values in ambient conditions [28, 34].

Here we determine the pressure variation of the full elastic stiffness tensor c_{ij} from direct computation of the stress tensors generated by small strains on the fully optimized cubic structure silicon with simultaneous ionic relaxation (table 1). Our calculated static values of c_{ij} at zero pressure are in excellent agreement with experimental [28] and previous pseudopotential [29–32] results (table 1). Both c_{11} and c_{12} increase monotonically with pressure whereas c_{44} increases initially followed by a gradual decrease with pressure. The diamond structure silicon exhibits high elastic anisotropy at zero pressure and the degree of the anisotropy increases with pressure (table 1).

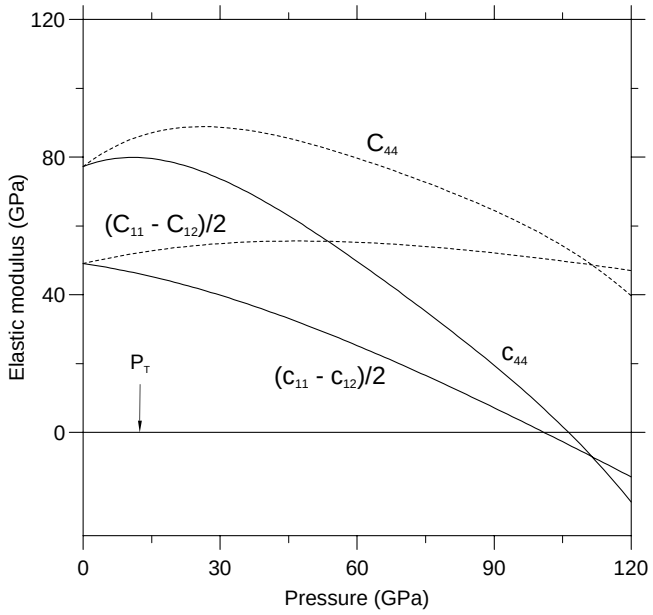

Figure 4. The pressure variation of different moduli for diamond structure Si.

As shown in figure 4, we find that the tetragonal shear modulus $((c_{11} - c_{12})/2)$ decreases gradually with pressure and vanishes at about 101 GPa, whereas c_{44} increases initially with pressure and soon starts to decrease finally to zero at the slightly higher pressure of 107 GPa. This implies that a tetragonal instability should occur at the much higher pressure of 101 GPa compared to the thermodynamic transition pressure in diamond structure Si in relation to the

observed diamond–β-Sn structural transformation as verified by the structural relaxation of the cubic lattice deformed with a small tetragonal strain. However, the conventional criteria in terms of elastic constants C_{ij} suggest that a shear instability ($C_{44} = 0$) would occur before the tetragonal instability ($(C_{11} - C_{12})/2 = 0$) at much higher pressures (figure 4), but the predicted instability ($C_{44} = 0$) is not associated with the cubic-to-tetragonal symmetry change of the transition. Kazuki *et al* [10] have also found that a tetragonal shear instability would occur and cause the diamond structure silicon to transform to the β-Sn structure at 105 GPa by using the appropriate elastic parameters, c_{11} and c_{12}, obtained from the values of the elastic constants (C_{ij}), using the Tersoff potential. The relatively much higher transition pressure for the transition from the diamond–cubic to the β-Sn structure suggested by elastic instability implies the existence of an activation barrier [10].

6. Discussion

We have examined four cases of transitions between phases related by continuous deformation. In each case, the elastic stiffness modulus associated with that deformation is observed to soften on approaching the transition and beyond.

In each case an elastic instability is predicted. In SiO_2 the instability occurs at the transition point in both high- and low-pressure phases, and we are justified in stating that the instability is the transition mechanism. In MgO, CaO and Si the elastic instability occurs only at pressures beyond that required for the transition—in these cases the transition mechanism is more complex than a simple elastic deformation, but the softening of the elastic moduli gives a strong hint as to the possibility of a phase transition.

There is an analogy here with the B_{1g} mode in SiO_2, which softens, though not to zero, on approach to the transition. Both softening phonon modes and softening elastic stiffnesses are indicators of an upcoming phase transition. This shows that instabilities predicted on the basis of the elastic criteria (equation (5)) formulated in terms of the elastic stiffness coefficients (c_{ij}) can be physically relevant.

The elastic predictions for the transition pressure differ significantly from the thermodynamic predictions in the cases of MgO, CaO and Si but the two types of prediction coincide for the case of silica. The B1–B2 phase transitions in MgO and CaO [12] and the diamond–β-Sn transition in Si [10] are of first order (a finite jump in volume at the transition) whereas the rutile-to-$CaCl_2$ phase transition in SiO_2 [14] is of second order (no discontinuity in the volume at the transition). This suggests that for the first-order phase transitions, the elastic stability does not imply thermodynamic stability, and hence the elastic stability criteria can determine only the pressure regimes where a given phase is stable or unstable with respect to a given elastic deformation, thus bounding the transition pressure from above and below.

Experimental observations of the first-order transitions tend to be close to the thermodynamic prediction since it is likely that the presence of any lattice defect in the real systems should destroy the constraints (the kinetic barriers) along the path of the homogeneous deformation [7, 10]. On the other hand, for the second-order phase transition, the predicted elastic instability actually drives the structural transformation and hence determines the transition pressure precisely.

For the case of isotropic stress, the elastic stiffness coefficients (c_{ijkl}) possess the full Voigt symmetry of the zero-stress elastic constants, i.e. c_{ijkl} is symmetric with respect to the index interchanges (i, j), (k, l), (ij, kl), and reduce both the equation of motion and stress–strain relations to the simple forms of the zero-stress case [8]. The elastic stiffness tensor, c_{ijkl} ($c_{\alpha\beta}$, in Voigt notation), are the appropriate elastic parameters which determine not only

the acoustic velocities and Cauchy relations but also determine the stability of a crystal under hydrostatic pressure. Moreover, although only hydrostatic pressure is investigated here, the elastic stability criteria expressed in terms of the elastic stiffness coefficients (c_{ijkl}) should provide a generalization of the stability criteria valid under arbitrary stress [6, 7].

Acknowledgments

The computing facilities are provided by the EPSRC under Grant GRIK74067. B B Karki acknowledges support from the University of Edinburgh under the Premier Scholarship. J Crain thanks the Royal Society of Edinburgh for support. The authors thank M C Warren, S J Clark and S Yip for useful discussion.

References

[1] Born M and Huang K 1954 *Dynamical Theory of Crystal Lattices* (Oxford: Clarendon)
[2] Hill R 1975 *Math. Proc. Cambridge Phil. Soc.* **77** 225
[3] Milstein F 1982 *Mechanics of Solids* ed H G Hopkins and M J Sewell (Oxford: Pergamon) p 417
[4] Hill R and Milstein F 1977 *Phys. Rev.* B **15** 3087
[5] Milstein F and Hill R 1979 *Phys. Rev. Lett.* **43** 1411
[6] Wang J, Yip S, Phillpot S R and Wolf D 1993 *Phys. Rev. Lett.* **71** 4182
[7] Wang J, Yip S, Phillpot S R and Wolf D 1995 *Phys. Rev.* B **52** 12 627
[8] Barron T H K and Klein M L 1965 *Proc. Phys. Soc.* **85** 523
[9] Wallace D C 1972 *Thermodynamics of Crystals* (New York: Wiley)
[10] Muzushima K, Yip S and Kaxiras E 1994 *Phys. Rev.* B **50** 14 952
[11] Tang M and Yip S 1995 *Phys. Rev. Lett.* **75** 2738
[12] Karki B B, Stixrude L, Clark S J, Warren M C, Ackland G J and Crain J 1997 *Am. Mineral.* **82** 51
[13] Karki B B, Clark S J, Warren M C, Hsueh H C, Ackland G J and Crain J 1997 *J. Phys. C: Solid State Phys.* **9** 375
[14] Karki B B, Warren M C, Stixrude L, Ackland G J and Crain J 1997 *Phys. Rev.* B **55** 3465
[15] Payne M C, Teter M P, Allan D C, Arias T A and Joannopolous J D 1992 *Rev. Mod. Phys.* **64** 1045
[16] Lee M H 1995 Advanced pseudopotentials for large scale electronic structure calculations *PhD Thesis* University of Cambridge, UK
[17] Lin J S, Qteish A, Payne M C and Heine V 1993 *Phys. Rev.* B **47** 4174
[18] Francis G P and Payne M C 1990 *J. Phys. C: Solid State Phys.* **2** 4395
[19] Monkhorst H J and Pack J D 1976 *Phys. Rev.* B **13** 5188
[20] Nielsen O H and Martin R M 1985 *Phys. Rev.* B **32** 3780
[21] Duffy T H, Hemley R J and Mao H K 1995 *Phys. Rev. Lett.* **74** 1371
[22] Warren M C and Ackland G J 1996 *Phys. Chem. Miner.* **23** 107
[23] Jeanloz R, Ahrens T J, Mao H K and Bell P M 1979 *Science* **206** 829
[24] Mammone J F, Mao H K and Bell P M 1981 *Geophys. Res. Lett.* **8** 142
[25] Richet P, Mao H K and Bell P M 1988 *J. Geophys. Res.* **93** 15 279
[26] Hu J Z, Merkel L D, Menoni C S and Spain I L 1986 *Phys. Rev.* B **34** 4679
[27] Chang K J and Cohen M L 1985 *Phys. Rev.* B **31** 7819
[28] McSkimin H J and Andreatch P Jr 1964 *J. Appl. Phys.* **35** 2161
[29] Nielsen O H and Martin R M 1985 *Phys. Rev. Lett.* **50** 697
[30] Wei S, Allan D C and Wilkins J W 1992 *Phys. Rev.* B **46** 12 411
[31] Shen S G 1994 *J. Phys. C: Solid State Phys.* **6** 8733
[32] Sandre G D, Colombo L and Bottani C 1996 *Phys. Rev.* B **54** 11 857
[33] Kingma M J, Cohen R E, Hemley R J and Mao H K 195 *Nature* **374** 243
[34] Donohue J 1974 *The Structures of the Elements* (New York: Wiley)